J Polym Res (2012) 19:9840
DOI 10.1007/s10965-012-9840-6

ORIGINAL PAPER

Extruded poly(ethylene-*co*-octene)/fly ash composites – value added products from an environmental pollutant

S. Anandhan · S. Madhava Sundar · T. Senthil · A. R. Mahendran · G. S. Shibulal

Received: 19 October 2011 / Accepted: 13 February 2012 / Published online: 4 March 2012

Abstract Fly ash (FA) is a by-product generated during combustion of coal and has caused serious environmental concerns. In an effort to utilize FA beneficially, we developed composites from an ethylene-octene random copolymer (EOC) and unmodified as well as surface-modified class-F fly ash (MFA) by twin screw extrusion. Addition of 20 wt% of MFA to EOC improves its tensile strength by 150%; also, MFA improves stress at 100% and 300% strains (M100 and M300) of EOC. Thermal stability of EOC matrix is appreciably improved by the addition of either FA or MFA, while the melting behavior is not appreciably influenced by either. Fractography study reveals an improved adhesion between the EOC and MFA particles up to a filler loading of 20%, beyond which the adhesion between EOC and MFA is weakened causing a reduction in mechanical properties. The 'flammable' nature of EOC changes to 'self extinguishing' on addition of even 10 wt% of FA or MFA, as found out from LOI study.

Keywords Fly ash · Surface modification · Ethylene-octene copolymer · Flammability · Thermal analysis

S. Anandhan (✉) · S. M. Sundar · T. Senthil
Department of Metallurgical and Materials Engineering,
National Institute of Technology-Karnataka,
Surathkal,
Mangalore 575025 Karnataka, India
e-mail: anandtmg@gmail.com

A. R. Mahendran
Kompetenzzentrum Holz GmbH,
W3C, A-9300 St. Veit/Glan, Klagenfurter Strasse 87-89,
Linz, Austria

G. S. Shibulal
Rubber Technology Center, Indian Institute of Technology,
Kharagpur 721302 W. Bengal, India

Introduction

Fly ash (FA), generated during the combustion of coal for energy production, is an industrial by-product and is an environmental pollutant. FA is commonly disposed off in dams and lagoons as landfill. This is not ideal, as FA is a mixture of alkali and transition metal oxides mainly of silicon, aluminium and iron, and small percentage of oxides of calcium, magnesium, potassium, sodium, titanium depending on the composition and processing of coal [1–4]. The present utilization of ash on worldwide basis varies widely from a minimum of 3% to a maximum of 57%, yet the world average only amounts to 16% of the total ash [5]. Thermal power plants are the main sources for power generation in India as well as many other countries. There are about 40 major thermal power plants in India and they have been generating about two thirds of the country's power demands. Chemical composition of FA varies depending upon type of coal used in combustion, combustion conditions and removal efficiency of air pollution control device. Because of the environmental concerns caused by FA, considerable research has been undertaken on the utilization and disposal of FA in an environment-friendly manner. FA has been used for many applications, such as brick making, manufacturing cement, polymer composites, etc. [5]. FA is being considered for use in composites with metals [6] and polymers. Polymers, in which FA has been used as filler include polyester [7, 8], epoxy [9], polypropylene [4, 10, 11], poly(vinyl alcohol) [3, 12, 13] and polyethylene [2, 14].

Polymer composites have been used in a variety of applications. Huge amount of literature is available on polymer composites. Still lot of researchers have been working on various composites based on a range of polymeric materials, such as plastics, rubbers and thermosets. Fillers used in

polymer composites can be either non-reinforcing or reinforcing ones. Non-reinforcing fillers are mostly added to polymers to reduce cost. They do not have any functional groups that can interact with polymers. Reinforcing fillers will interact chemically or physically with polymer chains to improve their tensile properties like tensile strength, modulus, hardness, etc.

The development of stronger interfacial bonds within composites can result in increased rigidity. In order to provide stronger interfacial interaction between filler and polymer, either polymer or filler may be functionalized.

Plastomer, a nomenclature constructed from the synthesis of the words plastic and elastomer, illustrates a family of polymers, which are softer (lower flexural modulus) than the common engineering thermoplastics such as polyamides, polypropylene, or polystyrene [15]. Structurally, plastomers straddle the property range between elastomers and plastics. Plastomers inherently contain some level of crystallinity due to the predominant monomer in a crystalline sequence within the polymer chains. ENGAGE™ [16], a commercially available ethylene copolymer with >25% of 1-octene content is a plastomer. Due to the saturated backbone of this polymer, it can be efficiently crosslinked by peroxide, irradiation or silane curing system.

EOC provides superb impact properties in blend with polypropylene and polyethylene, especially applications requiring slightly higher melt flow. EOC also provides high filler loading capability, excellent electrical properties and weathering resistance. It is used in applications, such as general purpose thermoplastic vulcanizates, impact modification and wires and cables [16]. In this study, we have developed composites from EOC and FA as well as MFA and studied their mechanical, thermal and flammability properties.

Experimental

Materials

Ethylene-octene random copolymer (ENGAGE™ 8200 with octene content of 38%) was kindly provided by Dow Elastomers, USA, through Bhimrajka Impex, India. It had a melt index of 5 dg/min at 190 °C/2.16 kg (ASTM D 1238); density 0.870 g/cm^3 (ASTM D 792); Mooney viscosity 8, ML_{1+4}@121 °C (ASTM D 1646); hardness 66 (shore A, 10 s ASTM D 2240-81). Class-F fly ash was provided by Thermal power station, Tuticorin, Tamil Nadu, India. Triethoxyvinylsilane (TEVS) was procured from Sigma-Aldrich, India. Methanol used as a medium for the surface treatment of fly ash was supplied by Nice chemicals, India.

Purification and sieving of fly ash

Loss on ignition measured by heating an accurately weighed fly ash sample in a muffle furnace at 800 °C for 3 h was 0.48%. Fresh fly ash was washed in distilled water and the carbon that creamed up during washing was removed. It was then dried at 110 °C for 48 h to remove water. Dried fly ash was sieved by using British standard sieves (BSS). Fly ash fraction that passed through 200 mesh but retained by 72 mesh was subjected to surface modification.

Surface modification of fly ash

10 g of TEVS was mixed with 100 g of methanol. 10 g of TEVS was used per 100 g of fly ash. The fly ash was mixed with the solution of TEVS in a polyethylene container with constant stirring to ensure uniform distribution of the coupling agent; mixing was continued for 30 min. The treated fly ash was then dried at 120 °C in a hot air oven for about 6 h to allow complete evaporation of the methanol.

Preparation of EOC/fly ash composites

Two sets of EOC composites containing 5, 10, 15, 20 and 25 wt% of FA and MFA were prepared by using a counter-rotating twin screw extruder (S. C. Dey and Co, Kolkata, India) at a screw rotation speed of 60 rpm. (Neat EOC is designated as EV000; EOC/FA composites are designated as EV001, EV002, EV003, EV004 and EV005; EOC/MFA composites are designated as MEV001, MEV002, MEV003, MEV004 and MEV005). The following temperature profile was used for mixing:

> Feed zone: 160 °C; transition zone: 180 °C; metering zone 3: 190 °C; die: 195 °C

The composites were compression molded in a hydraulic press (S. C. Dey and Co, Kolkata, India) between PET release films at 75 °C and 25 kN for 3 min. After 3 min, the load was released and the mold was removed and quenched in water. The molded sheets were then removed from the mould and trimmed; they were conditioned for 24 h at 25±2 °C prior to mechanical testing.

Characterization of fly ash and composites

Fourier Transform Infra red spectroscopy

FA was mixed with KBr and made into a pellet by using a hydraulic press. The FTIR spectrum of this pellet was taken in transmission mode by using a FTIR spectrometer (Thermo, Nicolet Avatar 330). The scans were made in a wave number range from 400 to 4000 cm^{-1} and the average of 32 scans was recorded.

X-ray diffraction of FA

The X-ray diffraction measurements were carried out for unmodified and modified fly ashes, with the help of a Goniometer (JEOL JDX 8P) using CuK_α radiation (λ=1.54056 Å) at an accelerating voltage of 30 kV and at a current of 20 mA. The samples were scanned at a speed of $1^{\circ}.min^{-1}$ in the range of 10–50°. Data analysis was done by using OriginPro® 8 software; the XRD spectra were smoothened by fast Fourier transform.

Scanning electron microscopy

Micrographs of FA and the composites were obtained by using a scanning electron microscope (JEOL-JSM-6380LA). FA was spread on the sample holder by a double sided carbon coated adhesive tape and then it was sputtered with gold (JEOL JFC 1600 auto fine coater) prior to analysis. To confirm the composition of the class-F fly ash, energy dispersive X-ray analysis (EDX) was performed (Link ISIS-300 Microanalytical System, Oxford lnstruments, UK). Prior to fractrography studies of the EOC/fly ash composites, the fracture surfaces were sputtered with gold.

Measurement of mechanical properties

Dumb-bell specimens of the control and composites were punched out by using an ASTM D412-B die from the molded sheets and the testing was done according to ASTM D418-98A using a universal testing machine (Hounsfield H10KS) at 25±2 °C at a constant cross head speed of 500 $mm.min^{-1}$. Properties such as tensile strength, yield strength, elongation at break, and stresses at 100% and 300% strain (denoted respectively as M100 and M300) were evaluated. 5 test specimens were used for testing and the averages of values have been reported. Maximum deviations in the results of tensile strength, yield strength M100, M300 and elongation at break were ±5%.

Differential scanning calorimetry

For DSC measurements, about 5 mg of the samples were heated in hermetically sealed aluminum pans kept in the furnace of the DSC analyzer (Mettler Toledo DSC) under a nitrogen atmosphere (flow rate: 50 $mL.min^{-1}$) from 0 to 100 °C at a heating rate of 10 $°C.min^{-1}$.

Thermogravimetry

For TG analysis, samples (8±0.2 mg) were heated from ambient temperature to 900 °C in a platinum crucible of the apparatus (TA Instruments, model Q5000, USA) at a heating rate of 10 $°C.min^{-1}$ under a dynamic air atmosphere flowing at 25 $mL.min^{-1}$.

Flammability study

The Limiting Oxygen Index (LOI) test is a widely used research and quality control tool for determining the relative flammability of polymeric materials. The LOI of the control and some representative composite samples was determined by using a Dynisco LOI analyzer according to ASTM D2863. A numerical index, the 'LOI', is defined as the minimum concentration of oxygen in an oxygen–nitrogen mixture, required to just support downward burning of a vertically mounted test specimen. Hence, higher LOI values represent better flame retardancy. LOI was calculated by using the following formula [17]:

$$LOI(\%) = \frac{[O_2]}{[O_2] + [N_2]} \times 100 \quad (1)$$

Where, $[O_2]$ is the volumetric flow rate of oxygen (cm^3/sec) and $[N_2]$ is that of nitrogen.

Results and discussion

Morphology of FA

The SEM micrograph of FA is shown in Fig. 1. Many spherical particles along with irregularly shaped ones are seen. Also, there is a wide distribution of particle size. The rounded particles with a wide distribution in size are predominantly glassy. The glass content in FA is generally higher than 70%. The angular particles are mostly comprised of crystalline solids, such as quartz, mullite, magnetite and hematite [18]. When the combined amount of the acidic oxides (silicon, aluminum and iron) is 70% or above, it is described as a

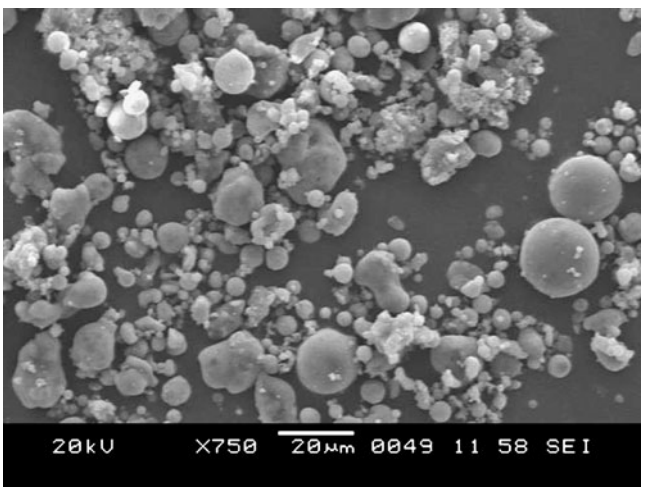

Fig. 1 SEM micrograph of FA showing the spherical glassy particles and irregular-shaped mineral particles

class-F ash. When this amount is between 50 and 70%, it is called a class-C ash [19]. The elemental composition of the FA was found out from SEM-EDX analysis and the averages of 10 values along with their respective standard deviations are given in Table 1. It is evident from the composition that the FA used in this research is a class- F ash.

FTIR spectroscopy

The FTIR spectra of the FA and MFA are shown in Fig. 2. Some important absorption bands characteristic of FA have been labeled. FTIR spectrum of FA shows four characteristic stretching vibration bands at 1067 and 798, 779 and 698 cm^{-1}. The stretching vibrations of Si–O–Al bonds occur mainly from 1,200 to 600 cm^{-1}. The strong and broad band at 1,067 cm^{-1} can be related to v3 (Si–O and Si–O–Al) asymmetric stretching vibration while 798 cm^{-1} band can be related to v4 (Si–O–Si) symmetric stretching vibration [20] as well as AlO_4 vibrations [21–23]. In the FTIR spectrum of MFA, two new peaks are seen at 2997 and 1656 cm^{-1}, which correspond to the C-H stretching vibration and C = C unsaturation of the vinyl group from the modifier TEVS [20]. This confirms that the modifier TEVS has successfully reacted with the surface OH groups of the fly ash components.

XRD results

The X-ray diffraction spectra of the FA and MFA are shown in Fig. 3, in which the mullite and quartz peaks have been labeled (by letters m and q respectively). There are no new peaks in the diffractogram of MFA in comparison with that of FA. So, it can be inferred that surface modification of FA with TEVS has not significantly affected the bulk properties of the FA.

Table 1 Composition and physical properties of fly ash

% Elemental Composition		% Oxide Composition	
Component	Content (%)	Component	Content (%)
Silicon	25.18±0.2	SiO_2	53.71±0.3
Aluminum	15.33±0.2	Al_2O_3	36.78±0.3
Iron	2.00±0.2	Fe_2O_3	4.79±0.2
Titanium	0.84±0.05	TiO_2	0.51±0.1
Potassium	0.73±0.06	K_2O	1.5±0.06
Sodium	0.41±0.1	Na_2O	0.82±0.1
Calcium	0.40±0.1	CaO	0.85±0.1
Magnesium	0.46±0.1	MgO	0.71±0.1
Oxygen	49.98±0.2	Total	99.67±0.3
Loss on ignition (%)			0.48
Density ($g.cm^{-3}$)			2.01

Mechanical properties

The tensile stress–strain curves of the EOC/FA and EOC/MFA composites are shown respectively in Figs. 4 and 5. Pristine EOC and all the composites exhibit similar stress–strain curves having an upper yield point. Neat EOC as well as all the EOC/FA and EOC/MFA composites (except MEV005) exhibit a very high elongation at break (>600%) that is characteristic of plastomers [15]. The variations in tensile strength, yield strength, M100 and M300 of EOC/FA and EOC/MFA composites as a function of filler volume fraction (φ) are shown in Figs. 6 and 7, respectively. In EOC/FA composites, the tensile strength decreases initially at a filler loading of 5% and then it reaches the maximum at a filler loading of 15%, beyond which it decreases again. There is no marked improvement in the tensile strength of EOC on addition of FA, which is not unexpected, because of dissimilar polarities of EOC and surface of FA particles. There is a marginal increase in yield strength up to a FA loading of 15%. M100 increases marginally with an increase in φ of FA, while M300 marginally decreases with an increase in φ. From the ongoing discussion, it can be understood that addition of FA to EOC does not cause any significant improvement in mechanical properties of EOC.

In EOC/MFA composites, the tensile strength increases proportionally to φ and there is an improvement by nearly 150% in tensile strength at a filler loading of 20%. Yield strength increases up to a filler loading of 15% beyond which it deteriorates. M100 and M300, which are considered as indicators of effective polymer-filler interaction in rubbery materials, increase continuously with φ and this indicates effective reinforcement of EOC by MFA.

To substantiate the effectiveness of interaction between EOC and MFA, an empirical equation put forward independently by Nielsen [24] and Smith [25] was employed in this study. For filler particles that have good adhesion with the polymer matrix, it was found that the elongation to break of the filled polymers, ε, follows

$$\varepsilon = \varepsilon_S(1 - \varphi^{\frac{1}{3}}) \quad (2)$$

Where, ε_s is the elongation to break of the unfilled polymer. If there is poor adhesion between fillers and the polymer matrix, the decrease in elongation to break with increasing filler loading is more gradual than that calculated from Eq. 2. However, there are cases where fillers promote craze formation that give rise to an increase in elongation to break with filler addition [26]. Elongation at break values of EOC/FA and EOC/MFA composites were calculated by Eq. 2, and have been plotted as a function of φ (Figs. 8 and 9). It can be seen from Fig. 8 that the decrease in elongation at break with increasing φ is more gradual than that calculated from Eq. 2, and it follows a linear trend. The experimental line is higher than the theoretical line. This

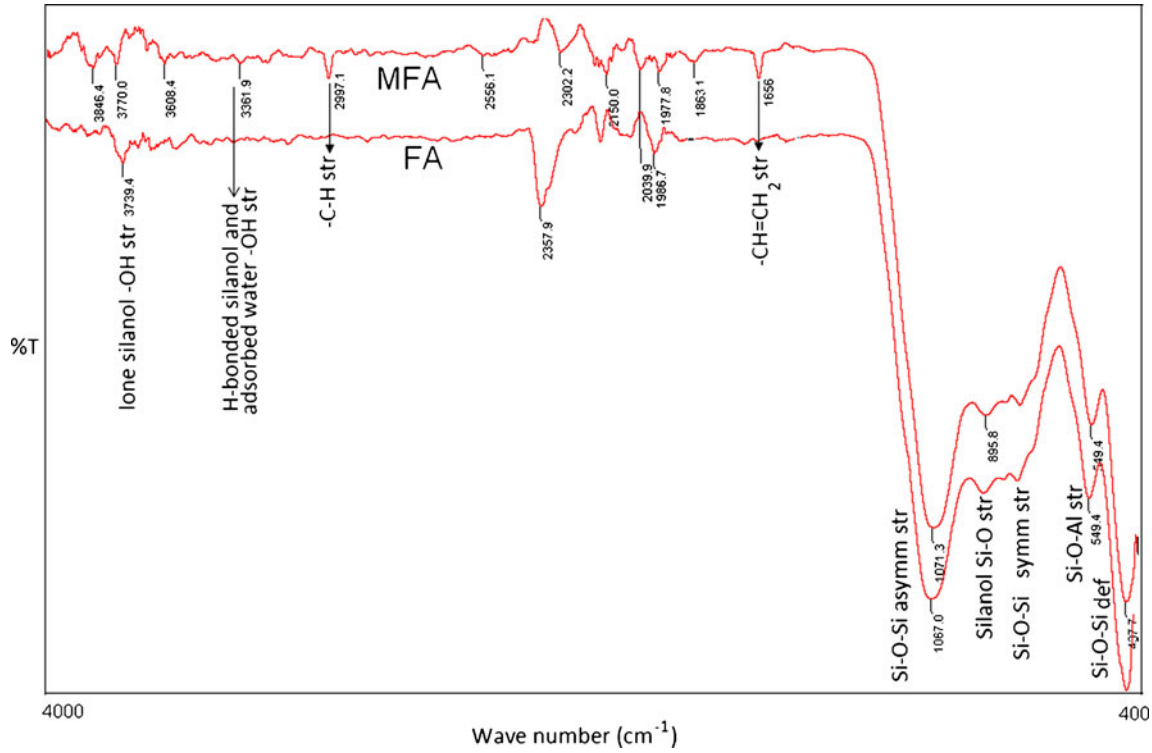

Fig. 2 FTIR spectra of FA and MFA

indicates a poor adhesion between FA particles and the EOC matrix. From Fig. 9 it is evident that there is an abrupt decrease in elongation at break of EOC/MFA composites with an increase in φ. Moreover, there is a very close match between theoretical and experimental values at filler loading of 15 and 20%. These observations as well as the graphical trend of other mechanical properties confirm an improved polymer-filler interaction in MFA/EOC composites (Scheme 1). However, there is a slight increase in elongation at break at filler loadings less than 15%. This observation can be justified on the basis of the explanation due to Nicolais and Narkis [26], who indicated that some fillers might promote craze formation in polymer matrix; and, that in turn, might give rise to an increase in elongation to break with filler addition. However, at present we could not provide any direct experimental evidence to corroborate this statement. At MFA loading of 25% there is a huge difference between experimental and theoretical values of elongation at break. This could be due to

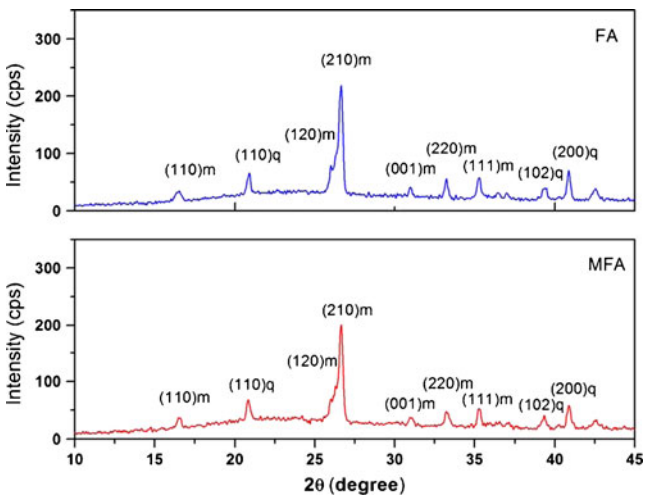

Fig. 3 XRD spectra of FA and MFA

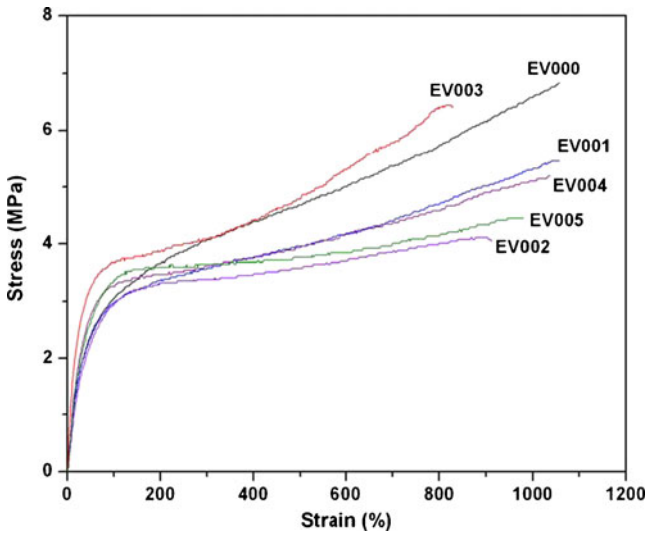

Fig. 4 Tensile stress versus strain curves of pristine EOC and EOC/FA composites

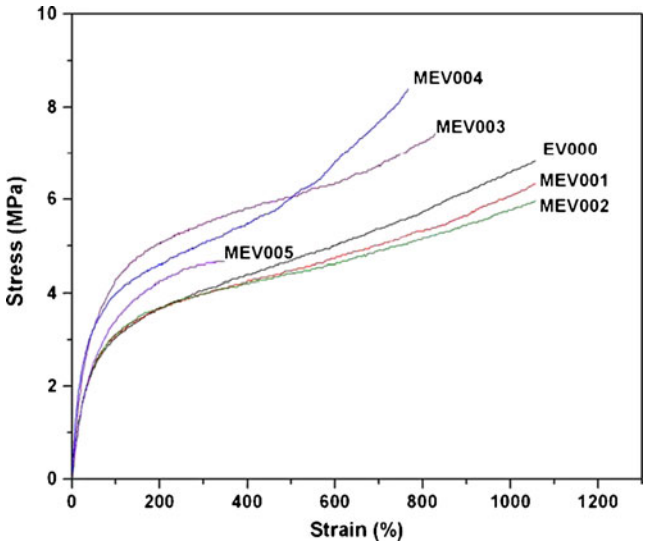

Fig. 5 Tensile stress versus strain curves of pristine EOC and EOC/MFA composites

dilution effect and thereby the MFA particles might have acted as flaws in the EOC matrix, reducing the elongation at break remarkably.

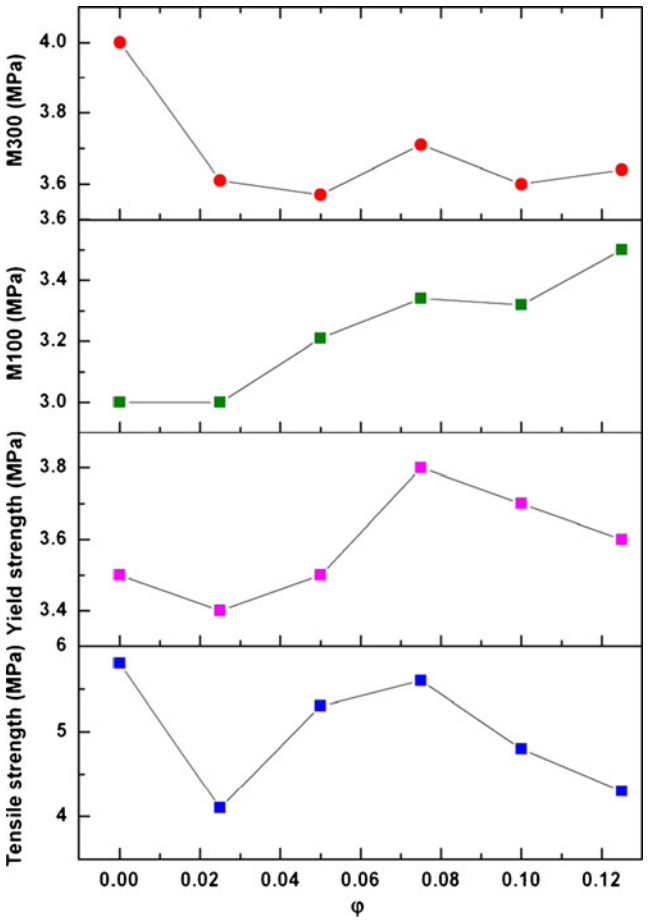

Fig. 6 Variation of mechanical properties of EOC/FA composites as a function of volume fraction of filler

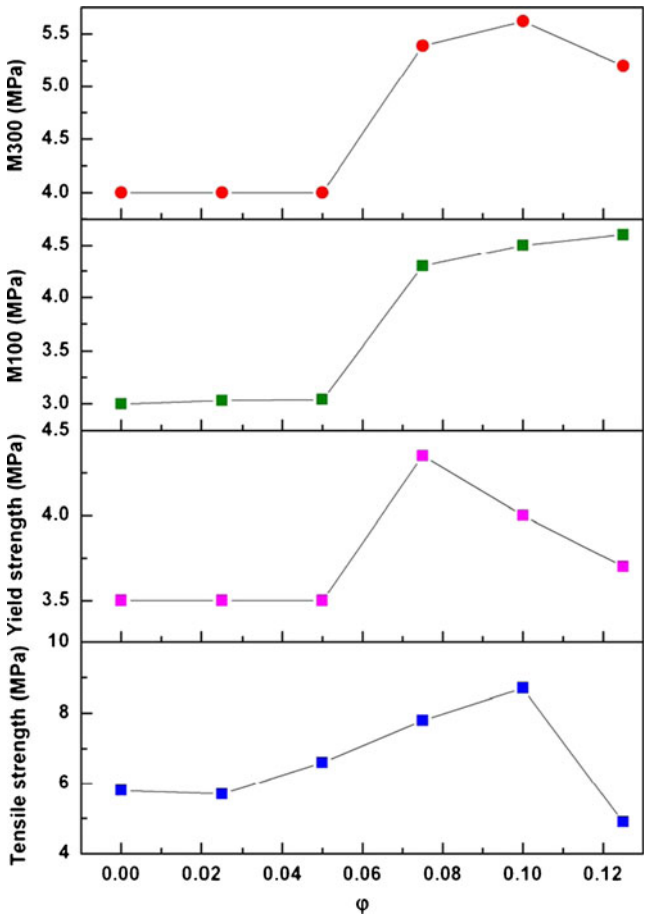

Fig. 7 Variation of mechanical properties of EOC/MFA composites as a function of volume fraction of filler

TGA results

TGA and DTG plots of pristine EOC and some representative EOC/FA and EOC/MFA composites are shown in Figs. 10 and 11, respectively; the onset (T_{onset}) and offset

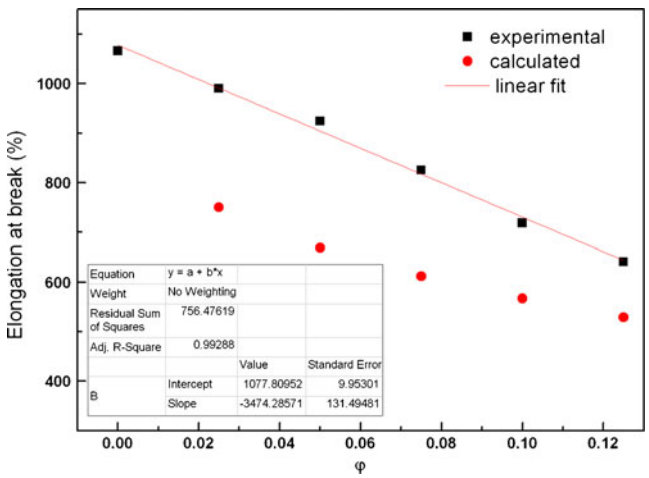

Fig. 8 Elongation at break versus volume fraction of filler of EOC/FA composites

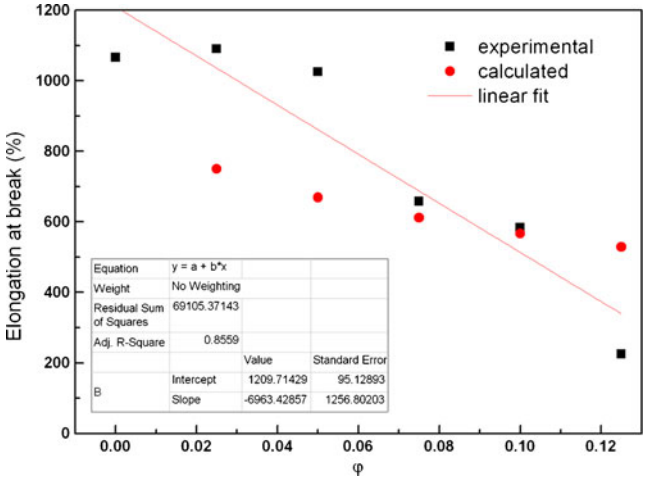

Fig. 9 Elongation at break versus volume fraction of filler of EOC/MFA composites

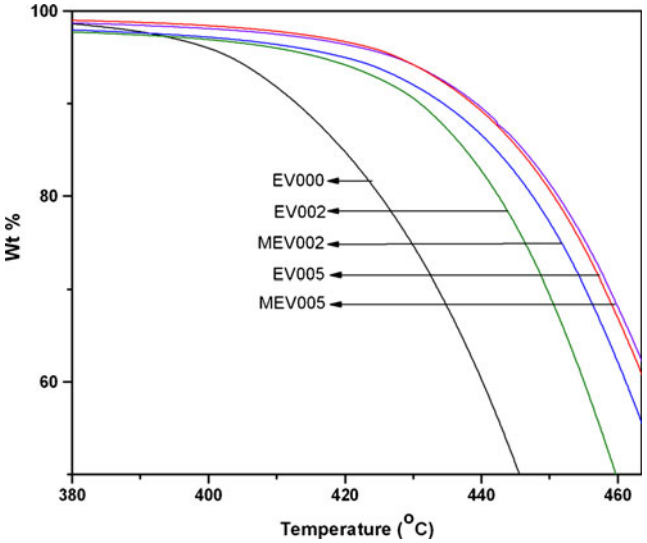

Fig. 10 TGA plots of pristine EOC, EOC/FA and EOC/MFA composites

(T_{offset}) temperatures of thermal degradation along with the temperature corresponding to the maximum rate of degradation (T_{max}) are shown in Table 2. Neat EOC and its composites with FA and MFA exhibit a single step degradation as can be seen from Fig. 11. There is an appreciable shift in T_{onset}, T_{offset} and T_{max} towards higher values on incorporation of either FA or MFA into EOC. The shift in these parameters towards higher temperatures is greater for the composites containing MFA.

DSC results

The DSC traces of the EOC/FA and EOC/MFA composites along with that of the neat EOC are shown in Figs. 12 and 13, respectively. EOC exhibits multiple melting peaks in its thermogram. This can be explained as follows: ethylene-octene copolymers possess only some residual crystallinity and that is due to ethylene sequences. Uninterrupted sequences of ethylene crystallize into periodic structures, which form crystalline lamellae. EOC contains 1-octene comonomer, which interrupts this sequencing of crystalline mers. 1-octene may be a monomer too large to fit into the crystal lattice. The residual hexyl side chain provides a site for the dislocation of the periodic structure required for crystals to be formed. Crystallization of the sequences occurs predominantly for longer sequences of monomers; shorter sequences of monomers cannot participate in crystal formation at ambient temperatures. It is believed that uninterrupted sequences of 12–20 monomers of ethylene are required for the formation of the most rudimentary crystals. Longer sequences lead to the formation of more robust structures. The loss of bulk crystallinity in EOC plastomers with increasing amounts of the comonomer is also accompanied by microscopic changes in the crystal structure. These changes affect the melting point of the crystals. While the unit cells of these crystalline structures are similar to the known crystal structure of the predominant monomer, the plastomer crystals are smaller, both due to thinner lamellae and due to lack of radial extension of the lamellae. The

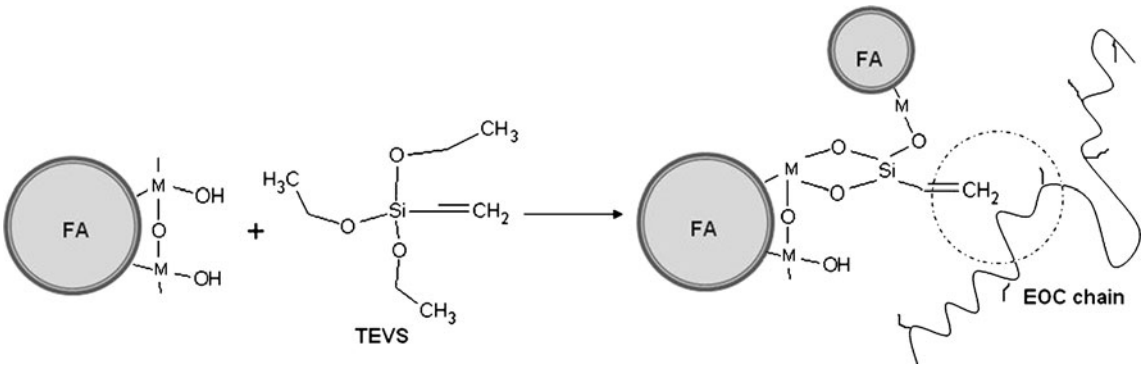

Scheme 1 Surface modification of FA and interaction of MFA with EOC polymer chain through nonpolar-nonpolar interactions

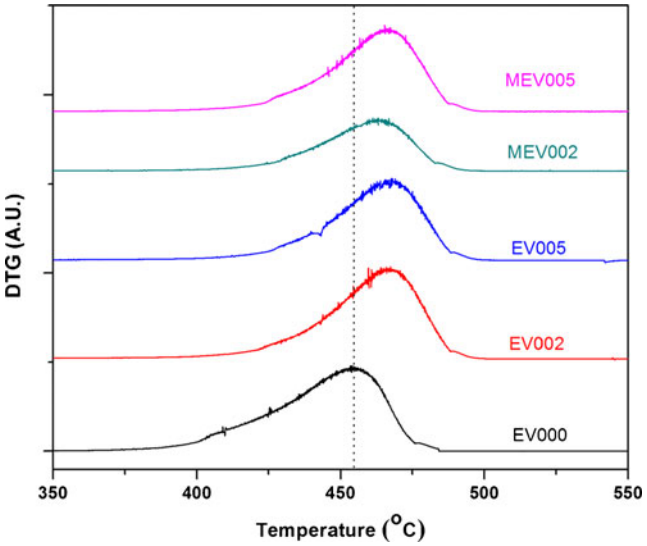

Fig. 11 Variation of rate of degradation of pristine EOC, EOC/FA and EOC/MFA composites as a function of temperature

lamellar dimensions decrease with increasing comonomer content, leading to increasing imperfection in the crystal structure [15]. This is the reason for the appearance of multiple melting endotherms in the DSC thermogram of plastomers such as EOC. From Figs. 12 and 13 it can be seen that there is no appreciable difference between the natures of the DSC traces of EOC and its composites with FA and MFA. Hence, we can conclude that addition of FA as well as MFA does not influence the melting and crystallization behavior of EOC.

Fractrography

Figure 14a shows the tensile fracture surface morphology of neat EOC. This seems to be a typical ductile failure. Figure 14b–f show the tensile fracture surfaces of EOC/FA composites. In all these micrographs loosely bound FA particles on EOC surfaces are seen. Also, there are holes corresponding to filler debonding due to dewetting of FA surface by EOC. This substantiates the necessity of improving the bonding between EOC matrix and FA particles by using a compatibilizer. Apart from these features, drawn fibrils of EOC can also be seen in the micrographs, which strongly suggest that the mode of failure in all these composites is ductile.

Figure 15a–e show the tensile fracture surfaces of EOC/MFA composites. In Fig. 15a–d, MFA particles covered by EOC matrix are seen. This suggests a strong interaction between MFA particles surfaces and EOC. Figure 15a–c shows yielded fibrils of EOC along with some striations that are typical of ductile failure in polymers. Figure 15d and e exhibit lot of holes and loose MFA particles along with those covered by EOC matrix. The elongated holes contain loosely held MFA particles, which are bigger in size indicating the possibility of them acting as flaws in the EOC matrix. These glassy particles are spherical in shape and are difficult to wet by EOC matrix; while the rough and irregularly shaped particles are seen to be firmly held by EOC matrix due to mechanical interlocking combined with the effect of compatibilization. It can be concluded that FA particle shape, size and surface modification are important in governing the adhesion between EOC matrix and FA particles.

Table 2 Results of TG analysis and LOI testing

Sample designation	T_{onset} (°C)	T_{offset} (°C)	T_{max} (°C)	LOI (%)
EV000	412	470	454	20
EV002	435	480	466	29
EV005	436	487	467	31
MEV002	435	482	463	29
MEV005	437	489	466	31

LOI results

The LOI values of neat EOC and some representative EOC/FA and EOC/MFA composites are shown in Table 2. It is seen that LOI of the composites improves by 50% even at a FA or MFA loading of 10 wt%. A higher loading of 25% of FA or MFA improves the LOI of the EOC matrix slightly higher than that of 10% filler loaded one. Several researchers have suggested that materials with a limiting oxygen index greater than 28 are generally self-extinguishing [27]. Thus, one can describe materials satisfying 28.00<LOI<100 as being "self-extinguishing" [28, 29]. EOC has a LOI of 20, thus it is a 'flammable' material. On incorporating 10 wt% of FA or MFA, its LOI attains a value of >28. Hence, the 'flammable' EOC becomes 'self-extinguishing' just by the addition of 10 wt% of FA or MFA. There is only a marginal improvement in LOI beyond this value on incorporating 25 wt% of either FA or MFA. This improvement in flammability of EOC is of great practical value from application point of view.

Conclusions

Surface modification of fly ash with TEVS was found to be effective in reinforcing some important mechanical parameters, such as tensile strength, yield strength, M100 and M300 of ethylene-octene copolymer. Surface-modified fly

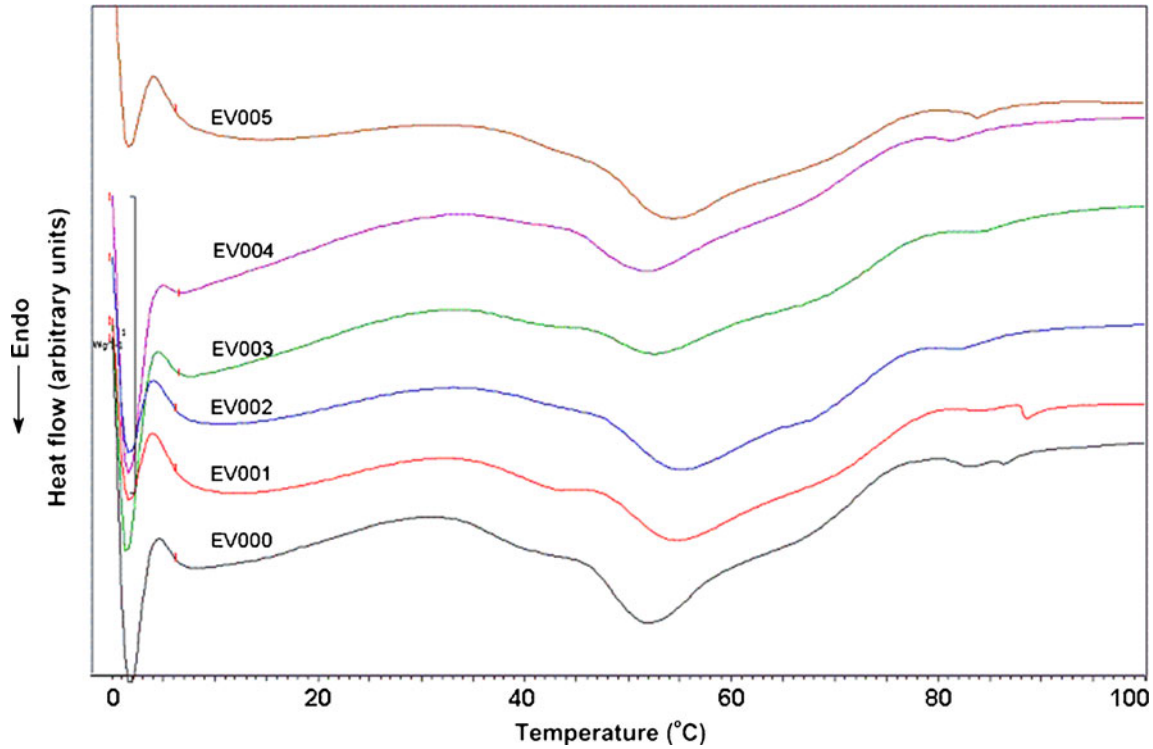

Fig. 12 DSC traces of pristine EOC and EOC/FA composites

ash could be used up to a loading of 20 wt% in ethylene-octene copolymer composites with an appreciable improvement in mechanical properties. Thermal stability and flammability of ethylene-octene copolymer are significantly improved by adding surface-modified fly ash. Both unmodified and surface-modified fly ashes do not seem to affect

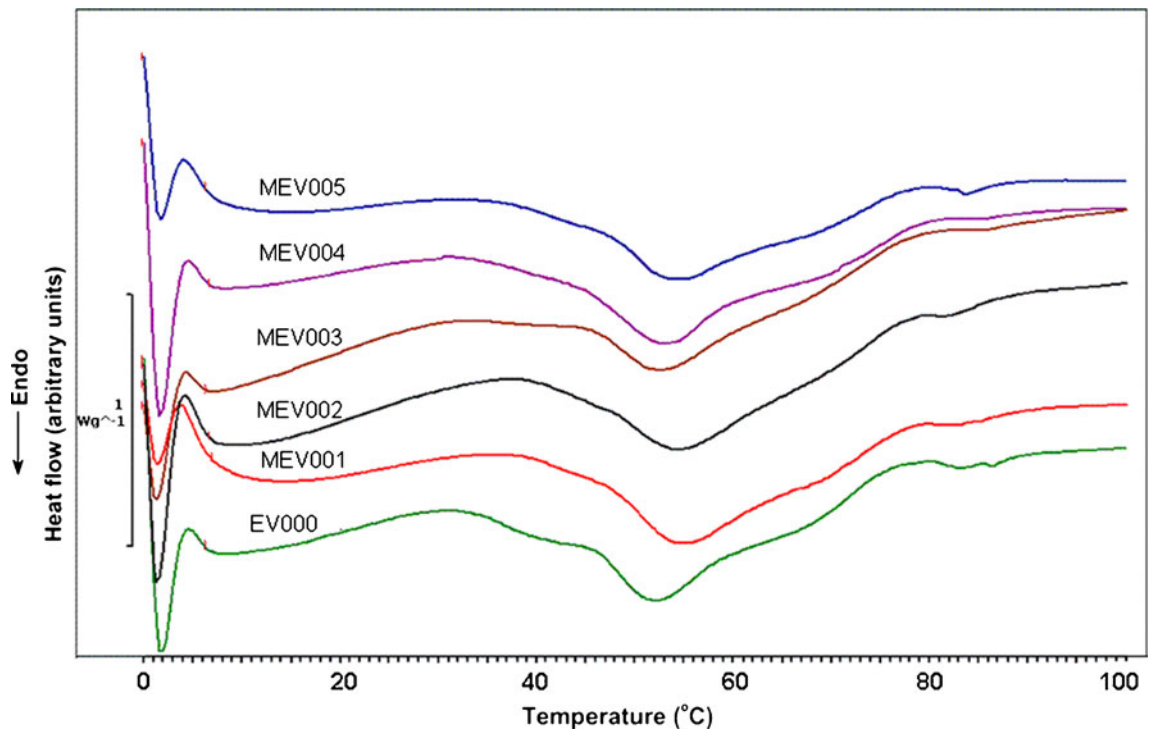

Fig. 13 DSC traces of pristine EOC and EOC/MFA composites

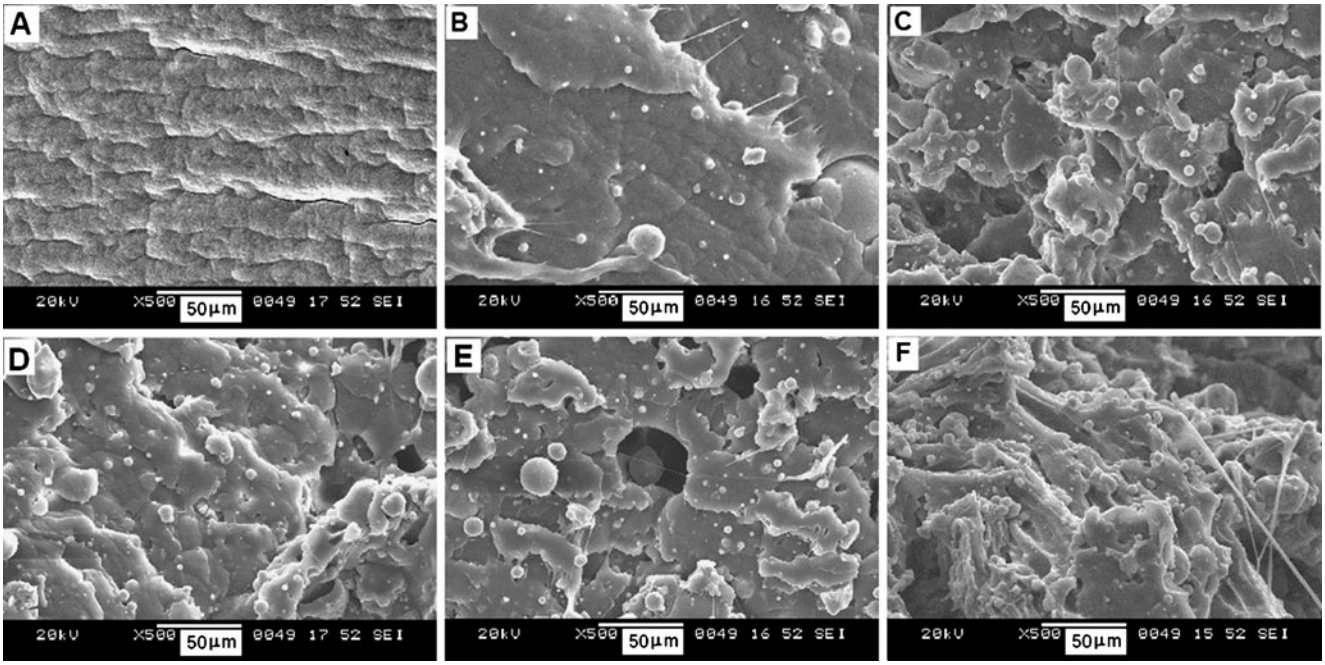

Fig. 14 SEM micrographs of tensile fracture surfaces of neat EOC and EOC/FA composites: **a**) EV000; **b**) EV001; **c**) EV002; **d**) EV003; **e**) EV004; **f**) EV005

the crystallization and melting behavior of ethylene-octene copolymer markedly. In summary, there is a huge potential for surface modified fly ash as filler for ethylene-octene copolymer, which is widely used in automobile and other commodity applications. Also, the use of surface-modified fly ash in ethylene-octene composites could be a means of beneficial way of utilization of fly ash, which is considered as an environmental pollutant.

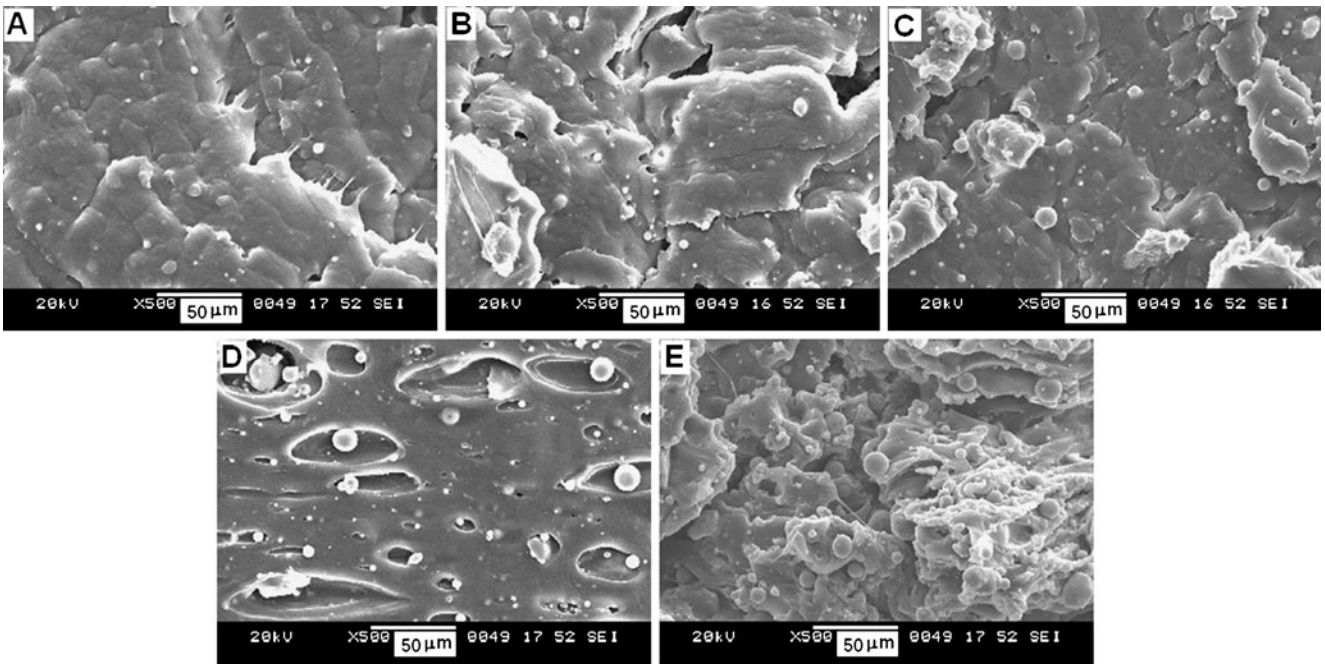

Fig 15 SEM micrographs of tensile fracture surfaces of EOC/MFA composites: **a**) MEV001; **b**) MEV002; **c**) MEV003; **d**) MEV004; **e**) MEV005

Acknowledgements The authors would like to thank Ms. U. Rashmi, Electron microscopy unit, NITK, for her assistance in scanning electron microscopy. Thanks are also due to Dow Elastomers, USA and Bhimrajka Impex, Mumbai, India for the supply of ENGAGE™ as a gift for our research.

References

1. Ward CR, French D (2006) Fuel 85:2268–2277
2. Alkan C, Arslan M, Cici M, Kaya M, Aksoy M (1995) Resour Conser Recyl 13:147–154
3. Nath DCD, Bandyopadhyay S, Boughton P, Yu A, Blackburn D, White C (2010) J Mater Sci 45:2625–2632
4. Nath DCD, Bandyopadhyay S, Yu A, Zeng Q, Das T, Blackburn D, White C (2009) J Mater Sci 44:6078–6089
5. Ahmaruzzaman M (2010) Prog Energ Combust Sci 36:327–363
6. Rajan TPD, Pillai RM, Pai BC, Satyanarayana KG, Rohatgi PK (2007) Comp Sci Technol 67:3369–3377
7. Guhanathan S, Sarojadevi M (2004) Comp Interface 11:43–66
8. Bishoyee N, Dash A, Mishra A, Patra S, Mahapatra SS (2010) J Polym Environ 18:177–187
9. Gupta N, Brar BS, Woldesenbet E (2001) Bull Mater Sci 24:219–223
10. Nath DCD, Bandyopadhyay S, Yu A, Blackburn D, White C (2010) J Appl Polym Sci 115:1510–1517
11. Nath DCD, Bandyopadhyay S, Yu A, Blackburn D, White C, Varughese S (2010) J Therm Anal Calorim 99:423–429
12. Nath DCD, Bandyopadhyay S, Boughton P, Yu A, Blackburn D, White C (2010) J Appl Polym Sci 117:114–121
13. Nath DCD, Bandyopadhyay S, Yu A, Blackburn D, White C (2010) J Mater Sci 45:1354–1360
14. Khan MJ, Al-Juhani AA, Shawabkeh R, Ul-Hamid A, Hussein IA, J Polym Res, 18:2275–2284
15. Datta S (2008) Plastomers. In: Bhowmick AK (ed) Current topics in elastomers research. CRC press, Boca Raton, pp 165–192
16. http://msdssearch.dow.com/PublishedLiteratureDOWCOM/dh_0132/0901b80380132265.pdf?filepath=elastomers/pdfs/noreg/774-00008.pdf&fromPage=GetDoc (accessed on 26 September 2011)
17. Chanda M, Roy SK (2009) Plastics: fundamentals, properties, and testing, first edn. CRC press, Boca Raton, pp 2-91–2-92
18. Mishulovich A, Evanko JL (2003) paper#18, 'Ceramic tiles from high-carbon fly ash', International ash utilization symposium, University of Kentucky
19. Designation: C618 – 08a, ASTM international, 2008
20. Smith B (1999) Infrared spectral interpretation—a systematic approach. CRC press, Boca Raton
21. Palomo A, Grutzeck MW, Blanco MT (1999) Cement Concr Res 29:1323–1329
22. Nath DCD, Bandyopadhyay S, Gupta S, Yu A, Blackburn D, White C (2010) App Surf Sci 256:2759–2763
23. Kaczmarek H, Podgorski A (2007) J Photochem Photobiol A 191:209–215
24. Nielsen LE (1966) J Appl Polym Sci 10:97–103
25. Smith TL (1959) Trans Soc Rheol 3:113–136
26. Nicolais L, Narkis M (1971) Polym Eng Sci 11:194–199
27. Horrocks AR, Tunc M, Price D (1989) Text Prog 18:1–205
28. Nelson MI (2001) Combust Theor Model 5:59–83
29. Nelson MI, Sidhu HS, Weber RO, Mercer GN (2001) ANZIAM J 43:105–117